



Picropodophyllin inhibits the growth of pemetrexed-resistant malignant pleural mesothelioma via microtubule inhibition and IGF-1R-, caspase-independent pathways

Rong Sun¹, Ryosuke Tanino¹, Xuexia Tong², Eshat Fahmida Haque¹, Yoshihiro Amano¹, Takeshi Isobe¹, Yukari Tsubata¹

¹Division of Medical Oncology & Respiratory Medicine, Department of Internal Medicine, Faculty of Medicine, Shimane University, Izumo, Japan;

²Department of Respiratory and Critical Care Medicine, General Hospital of Ningxia Medical University, Yinchuan, China

Contributions: (I) Conception and design: R Sun, R Tanino, T Isobe, Y Tsubata; (II) Administrative support: R Tanino, T Isobe, Y Tsubata; (III) Provision of study materials or patients: R Tanino, T Isobe, Y Tsubata; (IV) Collection and assembly of data: R Sun, R Tanino, X Tong, EF Haque, Y Amano; (V) Data analysis and interpretation: R Sun, R Tanino; (VI) Manuscript writing: All authors; (VII) Final approval of manuscript: All authors.

Correspondence to: Ryosuke Tanino, PhD. Division of Medical Oncology & Respiratory Medicine, Department of Internal Medicine, Faculty of Medicine, Shimane University, 89-1 Enya, Izumo, Shimane 693-8501, Japan. Email: rtanino@med.shimane-u.ac.jp.

Background: Acquired pemetrexed resistance leads to treatment interruption in patients with malignant pleural mesothelioma (MPM). Insulin-like growth factor-I receptor (IGF-1R) inhibitor is a candidate for treating pemetrexed-naïve MPM. However, the efficacy of cytotoxic and targeted drugs in acquired-pemetrexed resistant MPM is unclear. We explored anticancer drugs, including the IGF-1R inhibitor picropodophyllin, against acquired pemetrexed-resistant MPMs.

Methods: Acquired pemetrexed-resistant human MPM cell lines, named as H2452/PEM and 211H/PEM after their parental lines H2452 and 211H, respectively, were established by exposure to pemetrexed *in vitro*. Picropodophyllin and siRNA for IGF-1R knockdown were used to evaluate the efficacy of IGF-1R inhibition. Immunofluorescence was used to evaluate microtubule localization. The efficacy of picropodophyllin was evaluated in 3-dimensional MPM models.

Results: The acquired pemetrexed-resistant MPM lines retained their resistance after the removal of culture treatment. IGF-1R levels in H2452/PEM cells were higher than those in H2452 cells but not in 211H/PEM cells compared to the respective parental line. Picropodophyllin induced sub-G1 arrest in H2452/PEM cells but induced G2/M phase arrest in 211H/PEM cells, leading to caspase-independent cell death in the two acquired pemetrexed-resistant MPM lines. Although picropodophyllin inhibited phosphorylation of IGF-1R, specific inhibition of IGF-1R by RNA interference did not reduce the viability of pemetrexed-resistant MPM lines. Additionally, picropodophyllin reduced the viability of both IGF-1R knockdown pemetrexed-resistant MPM cells. Picropodophyllin was cytotoxic in acquired-pemetrexed-resistant MPM lines because of inhibition of microtubule formation and induction of aberrant mitosis. Moreover, combination treatment with picropodophyllin and vinorelbine synergistically affected the pemetrexed-resistant MPM lines but not the parental lines. Furthermore, we observed a similar efficacy of picropodophyllin in 3-dimensional pemetrexed-resistant MPM models.

Conclusions: Picropodophyllin may offer novel therapeutic properties for treating acquired pemetrexed-resistant MPM. Targeting tubulin may be an important strategy in the treatment of MPM after the discontinuation of pemetrexed.

Keywords: Malignant pleural mesothelioma (MPM); pemetrexed; acquired resistance; insulin-like growth factor 1 receptor inhibitor; microtubule

Submitted Oct 04, 2021. Accepted for publication Mar 13, 2022.

doi: 10.21037/tlcr-21-765

View this article at: <https://dx.doi.org/10.21037/tlcr-21-765>

Introduction

Malignant pleural mesothelioma (MPM) is a rare but aggressive cancer with a long latent period of up to 50 years after exposure to asbestos (1,2). Most patients with MPM are diagnosed at an advanced stage, and the 5-year survival rate is less than 10% (3). The use of asbestos, which is prevalent in some developing countries, may lead to an MPM epidemic because of the long latency of asbestosis (4,5).

Compared with standard chemotherapy, dual immunotherapy with nivolumab and ipilimumab was reported to improve the overall survival of patients with previously untreated, unresectable MPM (6). Nonetheless, 61% of patients experienced disease progression that led to death within 2 years (6). Moreover, immunotherapy is not suitable for patients with a poor performance status, autoimmune disease, or severe interstitial lung disease. The standard first-line chemotherapy, pemetrexed (PEM) plus platinum, continues to be used with other therapies for advanced MPM (7). Importantly, maintenance of PEM is also common in second-line treatment (7,8). However, long-term PEM therapy promotes acquired PEM resistance. Thus, additional therapeutic options are needed for MPMs with acquired PEM resistance.

Comprehensive genomic studies using The Cancer Genome Atlas revealed frequent deletions or loss-of-function mutations in tumor suppressor genes in patients with MPM. Patients with variants in cyclin-dependent kinase inhibitor 2A, BRCA1 associated protein-1 (BAP1), neurofibromatosis type 2, and TP53 in MPM were found to be difficult to treat, in contrast to patients with oncogene-driven mutations who can benefit from most molecular targeted drugs (9-11). Thus, preclinical, targeted drug studies have focused on the fibroblast growth factor receptor, focal adhesion kinase, mesothelin, and poly(ADP-ribose) polymerase (PARP) in MPM cells (12-15). However, molecular target therapy is not recommended for MPM because of its lack of efficacy in clinical trials (16,17).

Established mesothelioma lines and early passage cells obtained from mesothelioma widely express insulin-like growth factor-I receptor (IGF-1R) (18). IGF-1R binds IGF-1, IGF-2, and insulin, resulting in activation of IGF-1R which leads to activation of the PI3K-AKT and RAS-MAPK pathways (19). IGF-1R inhibitors, including monoclonal antibodies and tyrosine kinase inhibitors (TKIs), are also being evaluated as candidate molecules against MPM. An ATP-competitive TKI, NVP-AEW541, inhibited cell growth in MPM by inhibiting IGF-1R and its

downstream pathway (20). The IGF-1R antagonist antibody cixutumumab showed antitumor efficacy in MPM (18,21). Another ATP competitive TKI, AG1024, inhibited the growth of MPM cells and sensitized them to cisplatin (22). These studies highlight the efficacy of IGF-1R targeted therapy in MPM. However, studies targeting molecules such as IGF-1R in MPMs with acquired PEM resistance are lacking.

In this study, we established two MPM cell lines with acquired PEM resistance to identify effective anticancer drugs, including the IGF-1R inhibitor picropodophyllin (23), against acquired PEM-resistant MPMs. Our findings may provide a novel therapeutic approach for MPMs with acquired PEM resistance. We present the following article in accordance with the Materials Design Analysis Reporting (MDAR) checklist (available at <https://tlcr.amegroups.com/article/view/10.21037/tlcr-21-765/rc>).

Methods

Cell lines and culture reagents

Two human MPM cell lines were obtained from the American Type Culture Collection (ATCC, Manassas, VA, USA) and used as parental cell lines. Only cells passaged fewer than 30 times in our laboratory were used. H2452 (CRL-5946; ATCC, RRID: CVCL_1553) is an epithelial type, and MSTO-211H (211H, CRL-2081; ATCC, RRID: CVCL_1430) is a biphasic type of MPM. The variant and copy number data of tumor-associated genes in the MPM lines were acquired from the Broad DepMap dataset (24) (Table S1). Two PEM-resistant lines, PC-9/PEM and A549/PEM, were previously established in our laboratory from their parental human lung adenocarcinoma cell lines PC-9 (RRID:CVCL_B260) and A549 (RRID:CVCL_0023), respectively (25). The lung adenocarcinoma cell lines were tested after their establishment and authenticated by the JCRB Cell Bank through genetic testing using the PowerPlex 16 STR System (Promega, Madison, WI, USA). The cells were cultured in RPMI-1640 medium (189-02145; Fujifilm Wako, Osaka, Japan) supplemented with 10% fetal bovine serum (Biowest, Nuaillé, France) and 50 µg/mL gentamicin (Nacalai Tesque, Kyoto, Japan) in a humidified incubator with 5% CO₂ at 37 °C. Methotrexate (S1210; Selleck, Houston, TX, USA), picropodophyllin (PPP) (S7668; Selleck), vinorelbine ditartrate (S4269; Selleck), and Q-VD-OPh (Tonbo, San Diego, CA, USA) were dissolved in dimethyl sulfoxide. PEM disodium hydrate (S7785; Selleck) and fluorouracil (Kyowa Kirin, Tokyo, Japan) were dissolved

in phosphate buffered saline (PBS).

Establishment of PEM-resistant human MPM cell lines

To establish PEM-resistant MPM lines, parental MPM cells were cultured in T-75 or T-25 tissue culture flasks (TPP, Trasadingen, Switzerland) in the continuous presence of PEM. The concentration of PEM in the medium was increased from 10 nM to 3 μ M, which was reported to be the maximum tolerable concentration, according to the area under the blood concentration–time curve in a phase I clinical trial (26). The cells (H2452, 12,000 cells/cm²; 211H, 7,000 cells/cm²) were seeded after each passage. The concentration of PEM was gradually increased when the cell growth interval from seeding to 70% confluence was shortened by more than 50% from the first interval for each concentration without obvious changes in the cell shape and increase in the number of floating cells. The cells were confirmed to be proliferative after the concentration of PEM was increased; otherwise, they were cultured with PEM at the concentration used in the previous step. Mycoplasma infection was tested using a Mycoplasma PCR Detection Kit (Abm, Richmond, BC, Canada). The H2452 and 211H cell lines were passaged approximately 50 times to establish the PEM-resistant human MPM cell lines H2452/PEM and 211H/PEM, respectively (Figure S1).

Cell viability assay for monolayer culture

Cells were seeded in a 96-well tissue culture plate containing 200 μ L of medium per well. Cell viability was determined by the WST-8 assay using Cell Counting Kit-8 (Dojindo, Kumamoto, Japan), according to the manufacturer's instructions. The absorbance at 450 nm was measured using a Tecan Sunrise microplate reader (Tecan, Männedorf, Switzerland). The absorbance of the samples was divided by that of the vehicle control to determine the relative cell viability.

Quantitative reverse-transcription PCR

Cells were harvested at less than 70% confluence and frozen at -80 °C. The cells were lysed immediately after thawing using the RNeasy Mini Kit (Qiagen, Hilden, Germany). Total RNA was extracted according to the manufacturer's instructions. cDNA was generated from the RNA via reverse transcription using ReverTra Ace qPCR RT Master Mix with gDNA Remover (Toyobo, Osaka, Japan) following

the manufacturer's instructions. The sequences of primers used for quantitative PCR (qPCR) are listed in Table S2. qPCR was performed using Thermal Cycler Dice Real Time System II (Takara Bio, Kusatsu, Japan) and KOD SYBR qPCR Mix (Toyobo) with incubation at 98 °C for 2 min and 40 cycles under the following conditions: 98 °C for 10 s, 60 °C for 10 s, and 68 °C for 1 min (genes for folate and multidrug resistance) or 68 °C for 30 s [receptor tyrosine kinase (RTK) genes]. The value for *GAPDH* expression was used to normalize the expression values for the target genes.

Phosphorylation antibody array for receptor tyrosine kinases

Cells were collected at less than 70% confluence and lysed. Human RTK Phosphorylation Antibody Array-Membrane (ab193662; Abcam, Cambridge, UK) was used to measure the phosphorylation of 71 RTKs according to the manufacturer's instructions. Chemiluminescence signals from the membranes were acquired using an Amersham ImageQuant 800 (Cytiva, Marlborough, MA, USA).

Immunoblot analysis of protein expression

Details on immunoblot analysis of protein expression are provided in the Appendix 1.

Analysis of apoptosis and necrosis

Cells in culture, administered the treatment, were harvested, centrifuged at 800 \times g for 5 min, and then washed with PBS. The cells were then stained with annexin V-FITC and propidium iodide using a Mebcyto Apoptosis Kit (Medical & Biological Laboratories, Tokyo, Japan) following the manufacturer's instructions. Flow cytometry was performed on a BD FACS Calibur (BD, Franklin Lakes, NJ, USA) with the BD CellQuest Pro software (BD, RRID:SCR_014489).

Cell cycle analysis

H2452 and 211H cells in culture were treated with PPP or PEM for the indicated time period and then incubated with a medium containing 10 μ M BrdU provided in the BrdU Flow Kit (BD) for 6 and 4 h, respectively. The cells were then stained according to the manufacturer's instructions. The cell cycle analysis was performed using BD FACS Calibur (BD) with the BD CellQuest Pro software (BD).

Senescence-associated beta-galactosidase staining

Cells in culture, administered the treatment, were collected, centrifuged at 800 ×g for 5 min, and then fixed with 10% formalin neutral buffer solution for 5 min at 20–25 °C. The cells were then stained using SPiDER-βGal (Dojindo) following the protocol for fixed cells according to the manufacturer's instructions. Flow cytometry was performed using CytoFlex (Beckman Coulter, Brea, CA, USA) and CytExpert (Beckman Coulter).

siRNA transfection

Pre-designed Silencer Select siTYMS#1 (s14538; Thermo Fisher Scientific, Waltham, MA, USA), siTYMS#2 (s14539; Thermo Fisher Scientific), siIGF1R#1 (s7211; Thermo Fisher Scientific), and siIGF1R#2 (s7212; Thermo Fisher Scientific) were used for knockdown of TYMS or IGF1R. Silencer Select Negative Control siRNA (4390843; Thermo Fisher Scientific) was used as a negative control for siRNA transfection. siRNA was dispersed in diluted ScreenFect A plus reagent (Fujifilm Wako) and incubated for more than 5 min. The cells were suspended in the medium, and the siRNA dispersion was mixed with the cell suspension at a final siRNA concentration of 12.5 nM. These cells were then seeded into a 96-well plate and 60-mm dish. Cells in the 96-well plate were incubated for 120 h (in the case of IGF1R knockdown), and their viability was measured using the WST-8 assay. Cells in the 60-mm dish were incubated for 120 h (in the case of IGF1R knockdown) or 48 h (in the case of TYMS knockdown), respectively, and then harvested for immunoblotting and WST-8 assays.

Immunofluorescence staining

Cells were seeded onto a coverslip (Matsunami, Osaka, Japan) coated with Cellmatrix Type I-C (Fujifilm Wako) placed in a 6-well plate. The cells were fixed with ice-cold methanol for 10 min, washed with PBS three times, blocked with 0.3% Triton X-100 (Merck, Darmstadt, Germany) and 10% Blocker BSA (10X) in PBS (Thermo Fisher Scientific) for 60 min at 20–25 °C, and incubated overnight with anti-α-tubulin antibody (sc-5286; Santa Cruz Biotechnology, Dallas, TX, USA, RRID: AB_628411) prepared in 10% Blocker BSA (Thermo Fisher Scientific) in PBS at 4 °C. Subsequently, the cells were washed with PBS three times and incubated with Alexa Fluor 488 conjugated anti-mouse IgG (H+L), F(ab')₂ fragment antibody (4408; Cell Signaling

Technology, Danvers, MA, USA) for 60 min at 20–25 °C. The cells were washed with PBS three times and mounted with nuclear staining using ProLong Diamond Antifade Mountant with DAPI (Thermo Fisher Scientific), and then the coverslip was placed on a glass slide. Fluorescence imaging was performed using a confocal laser scanning microscope FV1000D (Olympus, Tokyo, Japan).

3D cell viability assay for spheroids

Cells in monolayer culture were collected at 70% confluence, suspended in 60 μL of medium, and seeded into the wells of PrimeSurface 96U (Sumitomo Bakelite, Tokyo, Japan) (H2452, 1,000 cells/well; 211H, 2000 cells/well; and 211H/PEM and H2452/PEM, 500 cells/well). Treatments were initiated after 72 h of culture to prepare stably formed spheroids. The spheroid cells were lysed using 50 μL CellTiter-Glo 3D Cell Viability Assay (Promega) by mixing with a pipette 10 times. The lysate was transferred into a white 96-well plate (Sumitomo Bakelite), shaken on a plate shaker for 5 min, and incubated in the dark at 20–25 °C for 25 min. Relative luminescence units were recorded using GloMax Discover (Promega) and standardized using the value for the vehicle control to indicate relative cell viability.

3D tumor model

Cells in monolayer culture were collected at less than 70% confluence. Cells suspended in 5 mL medium were seeded into a PrimeSurface Dish 60 (Sumitomo Bakelite) (H2452, 1×10⁶ cells/well; H2452/PEM, 5×10⁵ cells/well; 211H and 211H/PEM, 1.5×10⁵ cells/well). Treatments were started after 72 h of culture to prepare scaffold-free 3D tumor models. Tumors were collected after the indicated treatments, fixed with 10% neutral-buffered formalin solution, and embedded in paraffin. Tumor slices (4 μm) were stained with hematoxylin and eosin.

Statistical analysis

Statistical analysis was performed using SPSS Statistics version 17.0 software (SPSS, Inc., Chicago, IL, USA, RRID:SCR_002865). Student's *t*-test was used to compare two groups. One-way analysis of variance with a *post-hoc* test was used to compare more than two groups. Results were considered as statistically significant when *P*<0.05.

Results

Comparison of PEM sensitivity between PEM-naïve and PEM-resistant MPMs

To compare the sensitivity of PEM-resistant and PEM-naïve MPM lines to PEM, we established PEM-resistant cell lines, H2452/PEM and 211H/PEM, from parental human MPM lines, H2452 and 211H, respectively. We confirmed the constitutive PEM resistance of the PEM-resistant lines. We performed cell viability and cell cycle analyses after treating the cells with PEM. PEM decreased the cell viability of PEM-naïve parental lines but not of PEM-resistant lines (*Figure 1A*). Moreover, PEM exerted different effects on the cell cycle in the parental lines by inducing apoptotic sub-G1 and G2/M phase arrest in H2452 cells and intra-S and G2/M phase arrest in 211H cells (*Figure 1B*). PEM had no effect on the cell cycle in both PEM-resistant lines (*Figure 1B*).

Next, we evaluated PEM-induced proapoptotic activity in MPM lines. PEM induced early apoptosis in both parental lines but not in PEM-resistant lines (*Figure 1C*). Moreover, PARP cleavage was increased in PEM-treated H2452 and 211H cells. Consistently, no increase in PARP cleavage was observed in the PEM-treated H2452/PEM and 211H/PEM cell lines (*Figure 1D*).

To evaluate PEM-induced cellular senescence, we measured SA- β Gal activity. Although PEM induced SA- β Gal activity in parental and resistant lines, SA- β Gal activity was higher in PEM-treated surviving parental MPM lines, and was particularly more apparent in 211H than in the PEM-resistant lines (*Figure 1E*). Thus, PEM primarily promoted apoptosis in H2452 cells and induced G2/M phase arrest with cellular senescence in 211H cells but not in the PEM-resistant lines. These results consistently indicate that H2452/PEM and 211H/PEM cells are resistant to PEM and exhibit different characteristics. Compared to the respective parental line, decreased apoptosis in H2452/PEM cells and decreased drug-induced senescence in 211H/PEM cells were found to show the greatest changes.

Long-term PEM treatment changed folate and multidrug resistance protein levels in MPMs

PEM has multiple targets among folate enzymes, namely thymidylate synthase (TYMS), glycinamide ribonucleotide formyl transferase, and dihydrofolate reductase (DHFR) (27,28). We compared the levels of folate enzymes, folate

transporters, and multidrug-resistance proteins, which were reported to contribute to the acquisition of PEM resistance in PEM-resistant cancer lines from the respective parental lines (25,29,30). Expression of *TYMS*, *DHFR*, *SLC19A1*, and ATP binding cassette subfamily C member 5 (*ABCC5*) was increased in both PEM-resistant lines compared to that in the parental lines (*Figure 1F* and *Figure S2A*). The levels of *DHFR*, *SLC19A1*, and *ABCC5* were increased in 211H/PEM cells but that of *SLC19A1* was decreased in H2452/PEM cells (*Figure 1G*). *TYMS* levels consistently increased in the two PEM-resistant MPM lines (*Figure 1G*). However, knockdown of *TYMS* did not resensitize H2452/PEM and 211H/PEM cells to PEM (*Figure 1H,1I*).

To confirm the multidrug resistance of the PEM-resistant MPM lines to folate-related and anti-cytidine drugs, we treated these cells with fluorouracil, methotrexate, and gemcitabine, which target *TYMS*, *DHFR*, and pyrimidine metabolism, respectively. H2452/PEM cells showed resistance to fluorouracil (*Figure S2B*), whereas 211H/PEM cells were resistant to methotrexate and gemcitabine (*Figure S2C,S2D*). These results indicate that H2452/PEM and 211H/PEM cells have different PEM resistance characteristics. In addition, although *TYMS* levels were increased in both MPM lines with acquired PEM resistance, targeting *TYMS* for resensitizing the cells to PEM would be challenging.

MPM subline with acquired PEM-resistance showed increased IGF-1R expression and phosphorylation with downstream AKT activation

To identify another molecular target protein from RTKs in MPM lines with acquired PEM resistance, we evaluated the expression of RTKs at the mRNA and protein levels. The expression of *IGF1R* and *PDGFRB* was higher in H2452/PEM cells than in H2452 cells (*Figure 2A*). In contrast, the expression of all RTK genes either decreased or remained unchanged in 211H/PEM cells compared to that in 211H cells (*Figure 2A*). To examine the phosphorylation status of these RTKs in H2452/PEM cells, we used a phosphorylation antibody array. Several RTKs, including IGF-1R, were phosphorylated in H2452/PEM cells but not in H2452 cells. However, *PDGFR β* was not phosphorylated in H2452/PEM cells (*Figure 2B*). We confirmed the overexpression and increased phosphorylation of IGF-1R in H2452/PEM cells using immunoblotting (*Figure 2C*).

Next, we evaluated the phosphorylation status of AKT and ERK, which are RTK downstream effectors. AKT was

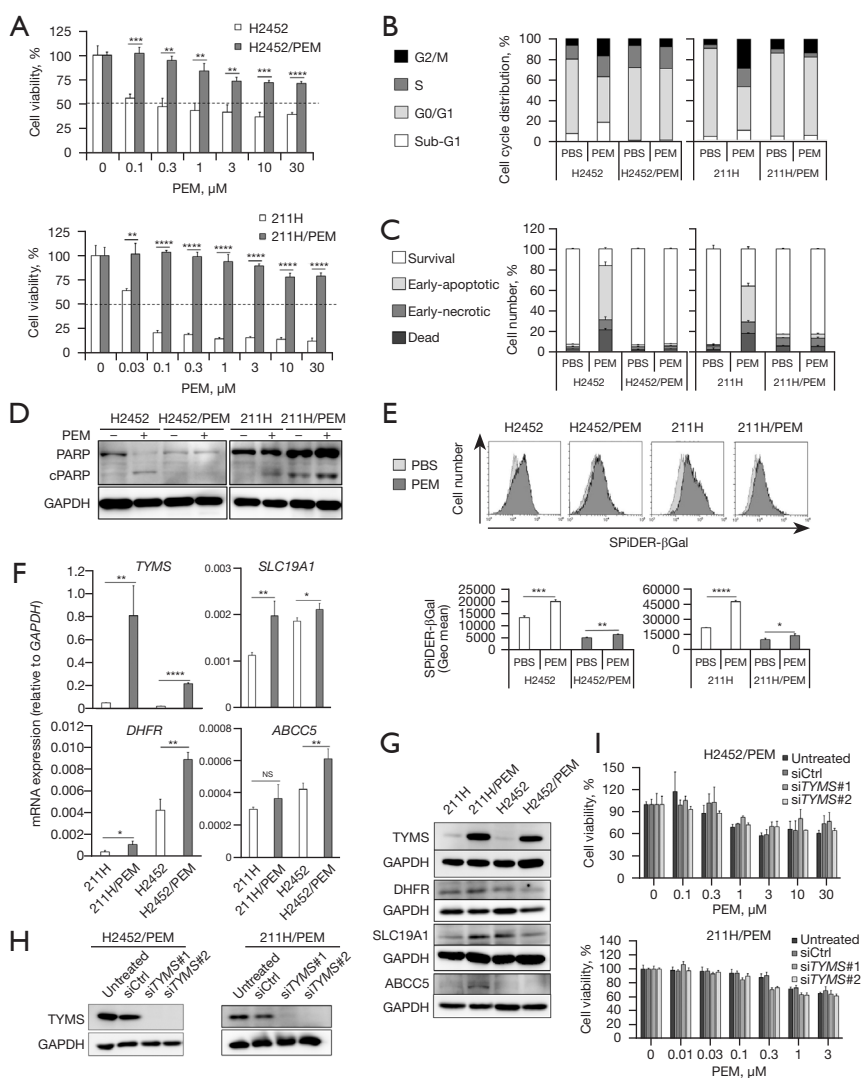


Figure 1 Two combinations of parental and pemetrexed (PEM)-resistant malignant pleural mesothelioma (MPM) cell lines. (A) Viability of MPM cells treated with the indicated concentrations of PEM for 144 h (H2452) or 96 h (211H) was determined using the WST-8 assay. Results represent the mean \pm SD, N=3 (biological replicates). P values were calculated using independent sample *t*-test: **, P<0.01; ***, P<0.001; ****, P<0.0001. (B) MPM cells were treated with 3 μ M (H2452) or 60 nM (211H) PEM for 96 h. Cell cycle analysis was performed after staining with BrdU and 7-AAD using flow cytometry. (C) MPM cells treated with 0.3 μ M PEM (H2452) or 60 nM PEM (211H) for 144 h (H2452) or 96 h (211H) were stained with annexin V/propidium iodide. Apoptosis assay was performed using flow cytometry. Results represent the mean \pm SD, N=3 (biological replicates). (D) Levels of PARP and cleaved PARP (cPARP) were analyzed by immunoblotting extracts of MPM cells treated with 3 μ M PEM (H2452) or 60 nM PEM (211H) for 96 h. (E) H2452 and 211H cells treated with 3 μ M PEM for 96 h were stained with SPiDER- β Gal. Fluorescence intensity was measured using flow cytometry. Results represent the mean \pm SD, N=3 (biological replicates). P values were calculated using the independent sample *t*-test: *, P<0.05; **, P<0.01; ***, P<0.001; ****, P<0.0001. (F) mRNA expression of thymidylate synthase (*TYMS*), dihydrofolate reductase (*DHFR*), solute carrier 19A1 (*SLC19A1*), and ATP binding cassette subfamily C member 5 (*ABCC5*) in MPM cells detected using quantitative reverse-transcription PCR. Results represent the mean \pm SD, N=3 (biological replicates). P values were calculated using the independent sample *t*-test: *, P<0.05; **, P<0.01; ****, P<0.0001. NS, not significant. (G) Levels of *TYMS*, *DHFR*, *SLC19A1*, and *ABCC5* in MPM cells evaluated using immunoblot analysis. (H) Levels of *TYMS* in H2452/PEM and 211H/PEM transfected with *TYMS* siRNA measured using immunoblot analysis. Untreated and negative control for siRNA transfection (siCtrl) were used. (I) Viability of *TYMS* knockdown H2452/PEM and 211H/PEM treated with PEM determined using the WST-8 assay. Results represent the mean \pm SD, N=3 (biological replicates).

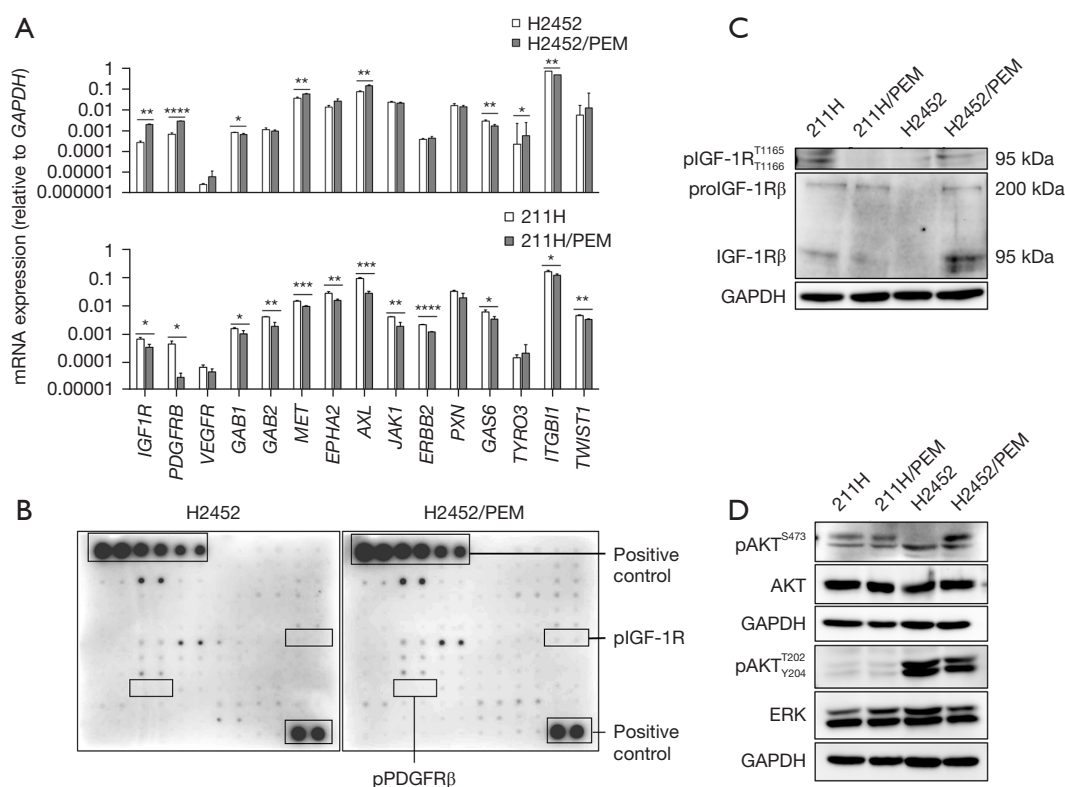


Figure 2 Increase in IGF-1R and phospho-IGF-1R levels in a pemetrexed (PEM)-resistant malignant pleural mesothelioma (MPM) subline, H2452/PEM. (A) mRNA expression of genes related to receptor tyrosine kinases in MPM cells detected using quantitative reverse-transcription PCR. Results represent the mean \pm SD, N=3 (biological replicates). P values were calculated using independent sample *t*-test: *, $P < 0.05$; **, $P < 0.01$; ***, $P < 0.001$; ****, $P < 0.0001$. (B) Phosphorylated human receptor tyrosine kinases were detected through phosphorylation antibody-array analysis of H2452 and H2452/PEM cells. (C) Levels of IGF-1R and phosphorylated IGF-1R in MPM cells were measured using immunoblot analysis. (D) Levels of AKT, phosphorylated AKT, ERK, and phosphorylated ERK in MPM cells were detected using immunoblot analysis.

more hyperphosphorylated in H2452/PEM cells than in H2452 cells (Figure 2D). In contrast, AKT and ERK were similarly phosphorylated to low levels in 211H and 211H/PEM cells (Figure 2D). The two PEM-resistant MPM lines showed different activation patterns in IGF-1R and downstream signaling.

PPP was more effective against MPM and non-small cell lung cancer lines with acquired PEM resistance, excluding A549/PEM, than the parental lines

Considering the overexpression of IGF-1R and increase in its phosphorylation levels in H2452/PEM cells, we evaluated the efficacy of PPP, a non-ATP competitive TKI for IGF-1R, which does not inhibit the insulin receptor, unlike other IGF-1R ATP competitive TKIs (23), against

MPM cells. First, we determined the viability of MPM lines treated with PPP (0.1–1.0 μ M) by determining the tolerated area under the blood concentration–time curve for 0–12 h in patients with non-small cell lung cancer (31). Unexpectedly, PPP decreased the viability of not only H2452/PEM cells but also 211H/PEM cells more than it decreased the viability of the parental lines (Figure 3A). Moreover, we measured the viability of PEM-resistant non-small cell lung cancer lines treated with PPP. PPP decreased the viability of PC-9/PEM cells to a greater extent than it did for PC-9 (Figure 3B). However, A549 and A549/PEM cells were resistant to PPP (Figure 3C). Cell cycle analysis revealed that PPP increased the proportion of H2452/PEM cells in the sub-G1 phase, and the proportion of 211H/PEM cells in sub-G1 and G2/M was greater than that of the parental lines (Figure 3D). In addition, PPP induced

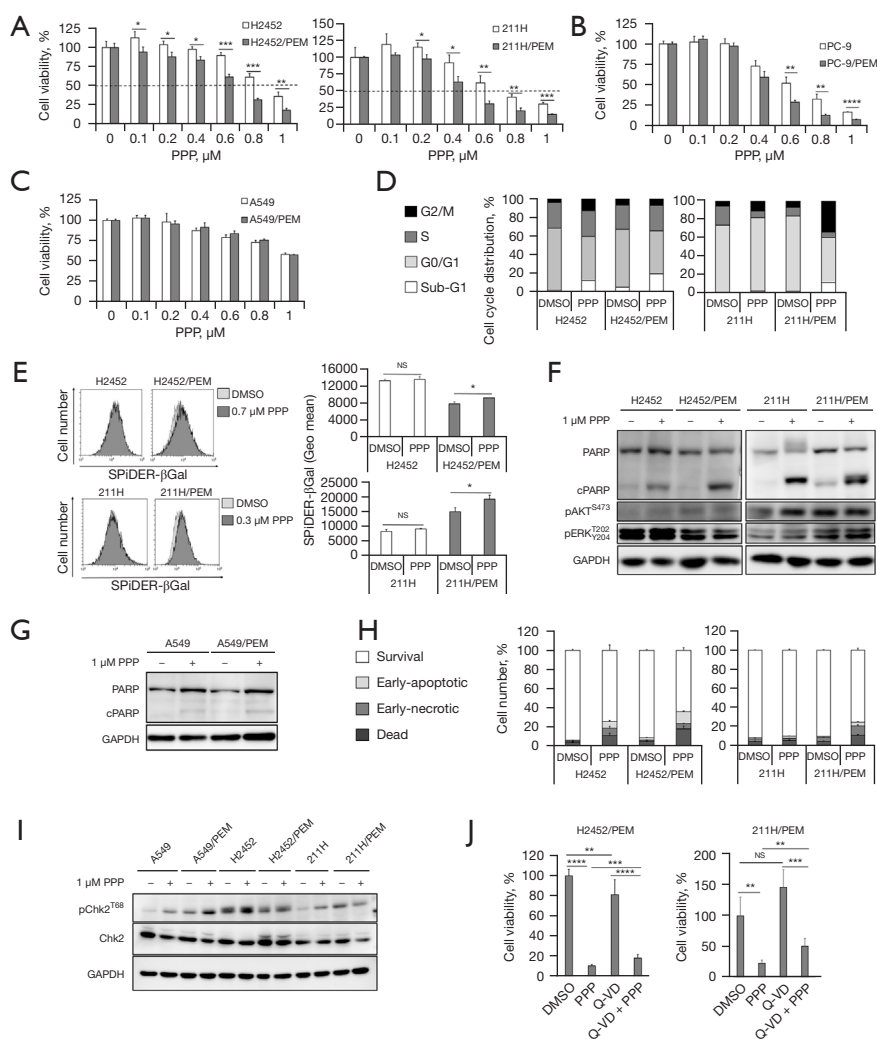


Figure 3 Evaluation of the efficacy of picropodophyllin (PPP) against four pemetrexed (PEM)-resistant cancer cell lines. (A) Viability of malignant pleural mesothelioma (MPM) cells treated with the indicated concentrations of PPP for 72 (H2452) or 48 (211H) h determined using the WST-8 assay. Results represent the mean ± SD, N=3 (biological replicates). P values were calculated using independent sample *t*-test: *, P<0.05; **, P<0.01; ***, P<0.001. (B) Viability of PC-9 cells treated with the indicated concentrations of PPP for 48 h was determined using the WST-8 assay. Results represent the mean ± SD, N=3 (biological replicates). P values were calculated using independent sample *t*-test: **, P<0.01; ****, P<0.0001. (C) Viability of A549 cells treated with the indicated concentrations of PPP for 72 h determined using the WST-8 assay. Results represent the mean ± SD, N=3 (biological replicates). (D) MPM cells were treated with 0.7 μM (H2452) or 0.6 μM (211H) PPP for 72 h (H2452) or 48 h (211H). Cell cycle analysis was performed using flow cytometry. (E) MPM cells treated with 0.7 μM (H2452, 72 h) or 0.3 μM (211H, 48 h) PPP were stained with SPIDER-βGal. Fluorescence intensity is measured using flow cytometry. Results represent the mean ± SD, N=3 (biological replicates). P values were calculated using independent sample *t*-test: *, P<0.05, NS, not significant. (F) Levels of PARP, cleaved PARP (cPARP), phospho-AKT, and phospho-ERK proteins in MPM cells treated with 1 μM PPP for 48 h (H2452) or 24 h (211H) measured using immunoblot analysis. (G) Levels of PARP and cPARP in A549 cells treated with 1 μM PPP for 72 h detected using immunoblot analysis. (H) MPM cells treated with 0.7 μM (H2452) or 0.6 μM (211H) PPP for 72 h (H2452) or 48 h (211H) were stained with annexin V/propidium iodide. Apoptosis assay was performed using flow cytometry. Results represent the mean ± SD, N=3 (biological replicates). (I) Levels of Chk2 and phospho-Chk2 in MPM and A549 cells treated with 1 μM PPP for 72 h measured through immunoblot analysis. (J) Viability of H2452/PEM (72 h) and 211H/PEM (48 h) cells treated with or without 1 μM PPP, 30 μM Q-VD-Oph (Q-VD), or 1 μM PPP and 30 μM Q-VD was determined using the WST-8 assay. Results represent the mean ± SD, N=4 (biological replicates). P values were calculated using one-way ANOVA and *post-hoc* Dunnett's test: **, P<0.01; ***, P<0.001; ****, P<0.0001. NS, not significant.

more senescence in both PEM-resistant MPM lines than in their respective parental lines (*Figure 3E*).

Next, we examined the levels of apoptosis-specific 89 kDa PARP fragment (cleaved PARP) (32) in PPP-treated cancer cells. The induction of cleaved PARP by PPP was higher in H2452/PEM cells than in H2452 cells and was equal in 211H and 211H/PEM cells (*Figure 3F*). However, PPP did not inhibit the phosphorylation of AKT and ERK in the MPM lines (*Figure 3F*). In contrast, the level of cleaved PARP in A549 and A549/PEM cells did not increase even when they were treated for a longer time than the other cells (*Figure 3G*). The apoptosis assay also showed that PPP treatment decreased the survival of 211H/PEM, H2452/PEM, and H2452 cells (*Figure 3H*). Moreover, PPP induced necrosis in both H2452/PEM and 211H/PEM cells (*Figure 3H*). Collectively, PPP was effective against cancer cells with acquired PEM resistance, excluding A549/PEM cells.

To determine whether PPP induces DNA damage before cell death in PEM-resistant lines, we evaluated the phosphorylation of Chk2. PPP did not induce DNA damage in PPP-sensitive PEM-resistant MPM lines. Although PPP induced DNA damage in PPP-resistant A549 and A549/PEM lines and the parental MPM lines (*Figure 3I*), it did not decrease the cell viability or induce apoptosis in these lines (*Figure 3C,3G*). The results indicate that DNA damage is not involved in the mechanism of PPP-induced cell death in the PEM-resistant MPM lines. We evaluated whether the death of cells without DNA damage was caspase-dependent. A pan-caspase inhibitor, Q-VD-OPh, did not rescue the effect of PPP in H2452/PEM and 211H/PEM cells (*Figure 3J*). In summary, PPP induced caspase-independent cell death without causing DNA damage in MPM cells with acquired PEM resistance.

IGF-1R inhibition does not lead to cytotoxicity in PEM-resistant MPM lines

Next, we evaluated the efficacy of IGF-1R inhibition by PPP in MPM lines with acquired PEM resistance. Lower concentrations of PPP decreased the levels of IGF-1R β in H2452/PEM (0.7 μ M) and 211H/PEM (0.6 μ M) cells but had no effect on its phosphorylation (*Figure 4A*). PPP (1.0 μ M) inhibited the expression and phosphorylation of IGF-1R in H2452/PEM cells after 72 h of treatment (*Figure 4B*). In addition, PPP (1.0 μ M) inhibited the phosphorylation of IGF-1R in 211H/PEM cells from 24 to 48 h of treatment (*Figure 4B*). In contrast, PPP (1.0 μ M) treatment did not

inhibit the phosphorylation and expression of IGF-1R in A549/PEM cells, which are resistant to PPP (*Figure 4B*).

To confirm whether the survival and growth of PEM-resistant MPM lines depends on IGF-1R, we knocked down *IGF1R*. Although the expression of IGF-1R β was significantly decreased (*Figure 4C*), the viability of H2452/PEM and 211H/PEM cells was not decreased (*Figure 4D*). Although si*IGF1R*#2 increased the viability of 211H/PEM cells, this was likely an off-target effect because inhibition of IGF-1R by si*IGF1R*#1 did not increase the viability of 211H/PEM cells (*Figure 4C,4D*). Moreover, after knockdown of *IGF1R*, PPP treatment decreased the viability of the PEM-resistant MPM lines (*Figure 4E*). Furthermore, knockdown of *IGF1R* did not re-sensitize H2452/PEM cells to PEM, indicating that the PEM resistance of H2452/PEM is not dependent on IGF-1R (*Figure S3*).

To evaluate dependence on other RTKs in PEM-resistant MPM lines, we used an EGFR-TKI, osimertinib, and multitarget TKI, nintedanib, which targets VEGFR, FGFR, and PDGFR. Unlike PPP, neither osimertinib nor nintedanib decreased the viability of parental and PEM-resistant MPM cells (*Figure S4A,S4B*). These results demonstrate that inhibition of neither IGF-1R nor of RTKs targeted by osimertinib and nintedanib was responsible for the anticancer effect of PPP in MPM lines with acquired PEM resistance.

Microtubules may be a critical factor for PEM-resistant MPMs

Considering the existence of another mechanism through which PPP inhibits microtubules (33,34), we examined the inhibition of microtubules after PPP treatment. Immunofluorescence analysis revealed that PPP induced the formation of mitotic spindles in H2452/PEM cells (*Figure 5A*). Multipolar spindles or spindle collapse were observed in H2452/PEM cells (*Figure 5B*). PPP increased the proportion of cytoplasmic microtubules (*Figure 5C*), resulting in cell rounding, indicating that microtubule depolymerization was inhibited (35) and multinucleation in 211H/PEM cells was induced (*Figure 5D*). In addition, PPP decreased the expression of α -tubulin in H2452/PEM cells but not in 211H/PEM cells (*Figure 5E*). These results demonstrate that PPP induced aberrant mitotic spindle organization in H2452/PEM cells and multinucleation in 211H/PEM cells.

We evaluated the sensitivity of MPM cells to other tubulin inhibitors. As observed for PPP, vinorelbine, a

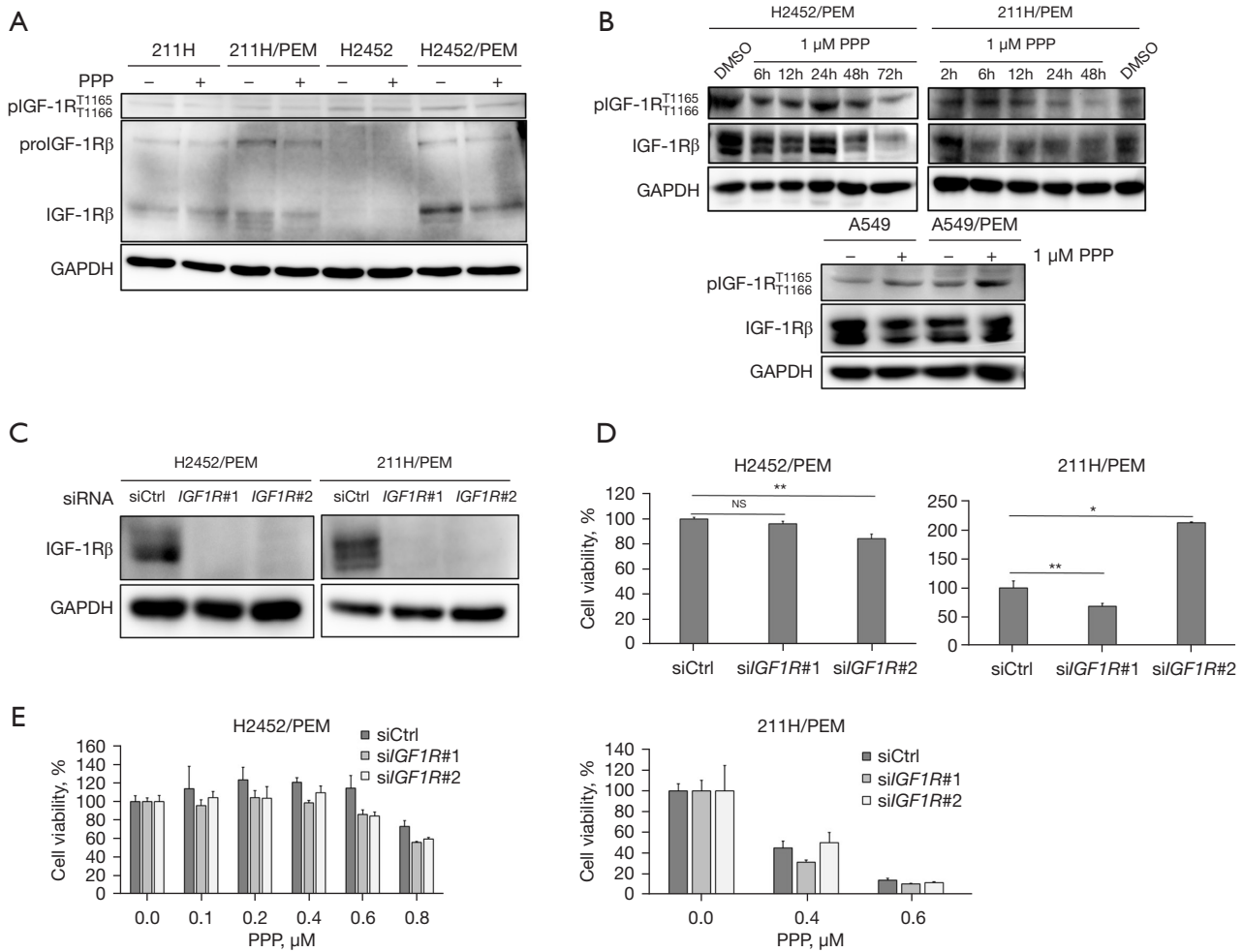


Figure 4 Evaluation of IGF-1R inhibition in pemetrexed (PEM)-resistant malignant pleural mesothelioma (MPM) cell lines. (A) Levels of IGF-1R and phospho-IGF-1R in MPM cells treated with 0.7 μ M picropodophyllin (PPP) for 72 h (H2452) or 0.6 μ M PPP for 48 h (211H) detected using immunoblot analysis. (B) Levels of IGF-1R β and phospho-IGF-1R in MPM cells treated with 1 μ M PPP for the indicated times measured using immunoblot analysis. Levels of IGF-1R β and phospho-IGF-1R in A549 cells treated with 1 μ M PPP for 72 h were detected using immunoblot analysis. (C) Levels of IGF-1R β in PEM-resistant MPM cells transfected with *IGF1R* siRNA measured using immunoblot analysis. Negative control for siRNA transfection (siCtrl) was used. (D) Viability of *IGF1R* knockdown PEM-resistant MPM cells determined using the WST-8 assay. Results represent the mean \pm SD, N=3 (biological replicates). P values were calculated using one-way ANOVA and *post-hoc* Dunnett's test: *, $P < 0.05$; **, $P < 0.01$. NS, not significant. (E) Viability of *IGF1R* knockdown PEM-resistant MPM cells treated with the indicated concentration of PPP for 72 (H2452/PEM) or 96 (211H/PEM) h. Negative control of siRNA transfection (siCtrl) was used. Results represent the mean \pm SD, N=3 (biological replicates).

microtubule destabilizing agent, decreased the viability of H2452/PEM cells to a greater extent than that of H2452 cells (Figure 5F). In contrast, the vinorelbine-induced decrease in cell viability was equal in 211H and 211H/PEM cells (Figure 5F). Paclitaxel, a microtubule-stabilizing agent, decreased the viability of H2452, 211H, and 211H/PEM cells. However, H2452/PEM cells were more resistant to

paclitaxel at 72 h of treatment than H2452 cells (Figure 5G). Although at 3 nM, paclitaxel had almost no effect on H2452/PEM cells at 96 h of treatment, 10 nM paclitaxel was sufficiently effective (Figure S5).

We assessed the efficacy of treatment with a combination of PPP and cytotoxic chemotherapeutic agents for MPM, including PEM, cisplatin, vinorelbine, and gemcitabine

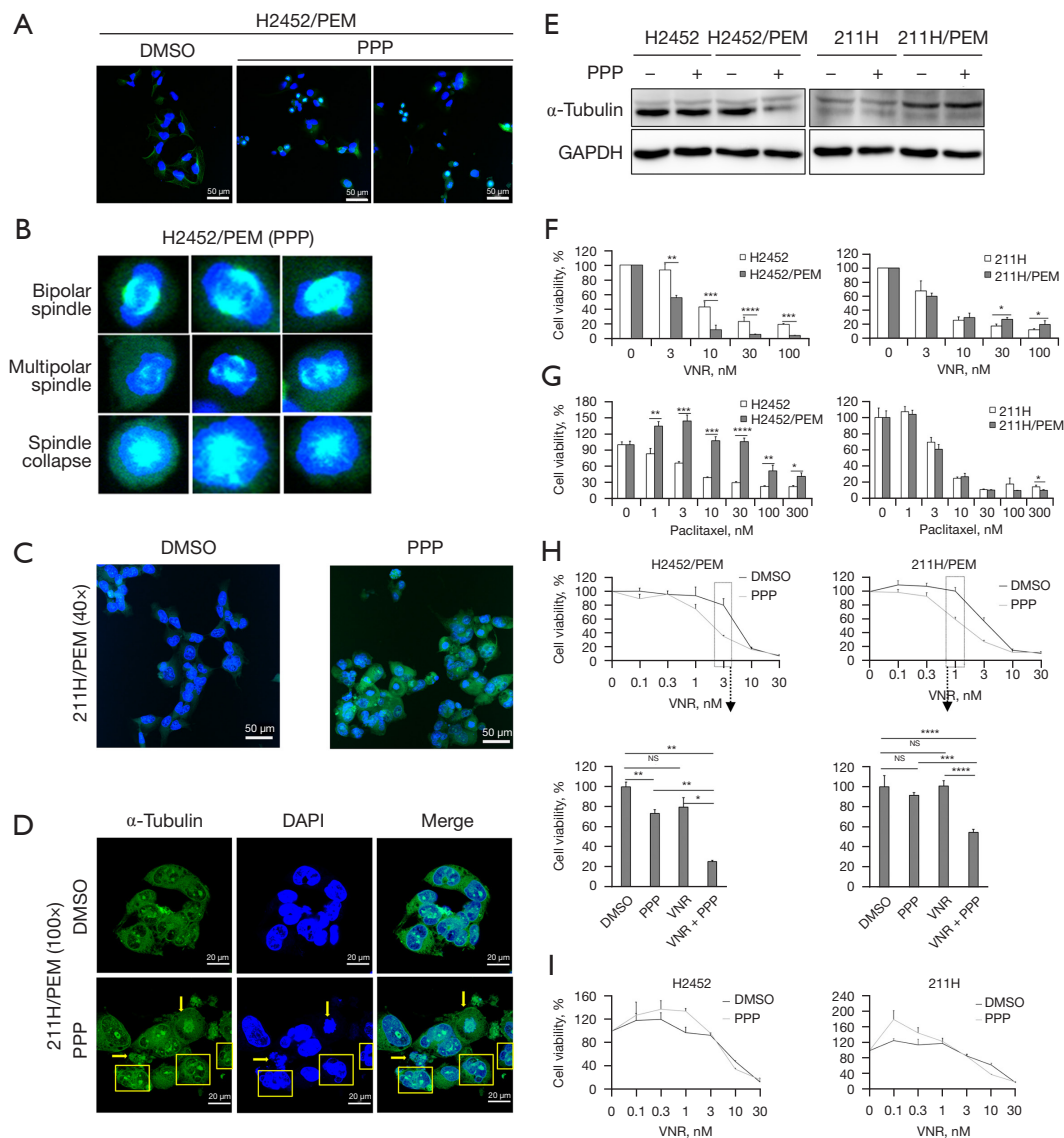


Figure 5 Picropodophyllin (PPP) inhibits microtubules, inducing aberrant mitosis in pemetrexed (PEM)-resistant malignant pleural mesothelioma (MPM) lines. (A,B) Images showing immunofluorescence of α -tubulin in H2452/PEM cells treated with 0.7 μ M PPP for 72 h. (B) Morphological organization of mitotic spindles. (C,D) Images showing immunofluorescence of α -tubulin in 211H/PEM cells treated with 0.6 μ M PPP for 48 h. (C) Confocal fluorescence images were obtained using the same settings for microscopy. (D) Arrows and boxes represent dead cells and multinucleation, respectively. (E) Levels of α -tubulin in MPM cells treated with 0.7 μ M PPP for 72 h (H2452) or 0.6 μ M PPP for 48 h (211H) measured using immunoblot analysis. (F) Viability of MPM cells treated with the indicated concentrations of vinorelbine (VNR) for 72 h determined using the WST-8 assay. Results represent the mean \pm SD, N=3 (biological replicates). P values were calculated using independent sample *t*-test: *, $P < 0.05$; **, $P < 0.01$; ***, $P < 0.001$; ****, $P < 0.0001$. (G) Viability of MPM cells treated with the indicated concentrations of paclitaxel for 72 h determined using the WST-8 assay. Results represent the mean \pm SD, N=3 (biological replicates). P values were calculated using the independent sample *t*-test: *, $P < 0.05$; **, $P < 0.01$; ***, $P < 0.001$; ****, $P < 0.0001$. (H) Viability of PEM-resistant MPM cells treated with the indicated concentrations of VNR without or with 0.5 μ M PPP for 72 h (H2452/PEM) or 0.3 μ M PPP for 48 h (211H/PEM) determined using the WST-8 assay. Results represent the mean \pm SD, N=3 (biological replicates). P values were calculated using one-way ANOVA and a *post-hoc* Dunnett's test: *, $P < 0.05$; **, $P < 0.01$; ***, $P < 0.001$; ****, $P < 0.0001$, NS, not significant. Similar results were obtained in two independent experiments. (I) Viability of MPM parental cells treated with the indicated concentrations of VNR without or with 0.5 μ M PPP for 72 h (H2452) or 0.3 μ M PPP for 48 h (211H) determined using the WST-8 assay. Results represent the mean \pm SD, N=3 (biological replicates).

(Figure S6A-S6D). Notably, PPP plus vinorelbine had a synergistic effect only in the PEM-resistant MPM lines (Figure 5H) but not in the parental lines (Figure 5I). Combinations of PPP with PEM, cisplatin, or gemcitabine had no synergistic effect in the two PEM-resistant MPM lines (Figure S6A-S6D). These results indicate that the mechanism of action of PPP differs from that of vinorelbine. Moreover, the PEM-resistant MPM lines may be more sensitive to tubulin targeting compared to the parental lines.

PPP was also effective in 3D MPMs

To confirm whether PPP is effective in 3D MPM cells, we established 3D MPM spheroids and 3D tumor models. PEM adversely affected the spheroid shape of both parental lines, but the PEM-resistant lines maintained a healthy spheroid shape, that is, they retained resistance in the spheroid form after acquiring this shape in monolayer culture (Figure 6A). Although PEM slightly decreased the 3D cell viability of PEM-resistant lines, spheroids of the parental lines were more susceptible to PEM than those of PEM-resistant lines (Figure 6B). In contrast, PPP decreased the spheroid size of H2452/PEM, 211H, and 211H/PEM cells but not of H2452 cells (Figure 6C). Consistent with results from monolayer culture, PEM-resistant lines were more sensitive to PPP than were parental lines in the 3D cell viability assay (Figure 6D).

Hematoxylin and eosin-stained 3D MPM tumor models showed healthy tumor growth in the control group (Figure 6E). PPP treatment decreased the tumor size and increased aberrant tumor formation, with less stained necrotic areas in the PEM-resistant tumor models (Figure 6E). However, the spheroids of parental MPM lines were not affected by PPP to the same extent as the PEM-resistant lines (Figure 6E). Thus, PPP exhibits anticancer effects in 3D PEM-resistant MPM cells.

Discussion

Our findings revealed that PPP was cytotoxic to MPM lines with acquired PEM resistance by inhibiting microtubule formation and not by IGF-1R inhibition alone. Moreover, PPP plus vinorelbine had a synergistic effect on MPM lines with acquired PEM resistance. PPP was also found to be effective against the 3D MPM tumor model. To our knowledge, this is the first report on PPP being an effective drug for MPM cell lines with acquired PEM resistance.

Furthermore, the synergistic effect of PPP plus vinorelbine against MPM cell lines with acquired PEM resistance was revealed in this study.

Inhibition of IGF-1R by IGF-1R TKIs, neutralizing antibodies, and antagonistic peptides is a therapeutic strategy for several cancers, including breast cancer, prostate cancer, colon cancer, multiple myeloma, and other solid tumors (36-39). The IGF-1R inhibitor NVP-AEW541 is effective in PEM-naïve MPM lines by inhibiting IGF-1R phosphorylation (20). However, we found that PPP had a slight anticancer effect only against PEM-naïve MPM lines, in contrast to its effect on the PEM-resistant lines. Moreover, siRNA-mediated inhibition of IGF-1R did not decrease the viability of PEM-resistant MPM cells, indicating that the efficacy of PPP on PEM-resistant MPM cells was not solely dependent on inhibition of IGF-1R. Concurrently, PPP induced the formation of multipolar spindles in H2452/PEM cells and multinucleation in 211H/PEM cells. These effects are considered as morphological features of drug-induced mitotic catastrophe (40). In accordance with these results, PPP was reported to directly inhibit microtubule polymerization (33) and induce microtubule depolymerization in the cell cycle (34). Unlike IGF-1R inhibition, mitotic catastrophe is not considered to be controlled by the apoptotic cell death pathway (41). Consistently, Q-VD-OPh did not rescue the viability of PPP-treated PEM-resistant MPM cells. In addition, PPP mainly induced sub-G1 arrest in H2452/PEM cells but G2/M phase arrest in 211H/PEM cells, indicating inconsistent characteristics between the two PEM-resistant MPM lines. The BAP1 and LATS1/2 genes are known as tumor suppressor genes of MPM (42-44), and variants of BAP1 and LATS1/2 were detected in H2452 and 211H cells, respectively. BRCA1, which was positively regulated by BAP1, was recently identified as a regulator of the spindle assembly checkpoint (45,46). In contrast, LATS1 and LATS2 are important for sensing mitotic stress (47). Variants of these genes may induce mitotic spindle formation instability through different mechanisms and inconsistent PPP-induced effects in 211H/PEM and H2452/PEM cells. However, the action mechanisms of microtubule inhibition remain unclear in PEM-resistant MPM and require further analysis.

We also demonstrated the anticancer effects of vinorelbine, a microtubule destabilizing agent which is one of the recommended drugs for MPM in clinical settings (48). We found that the anticancer effects of PPP were stronger in combination with low concentrations of vinorelbine in MPM lines with acquired PEM resistance. These data

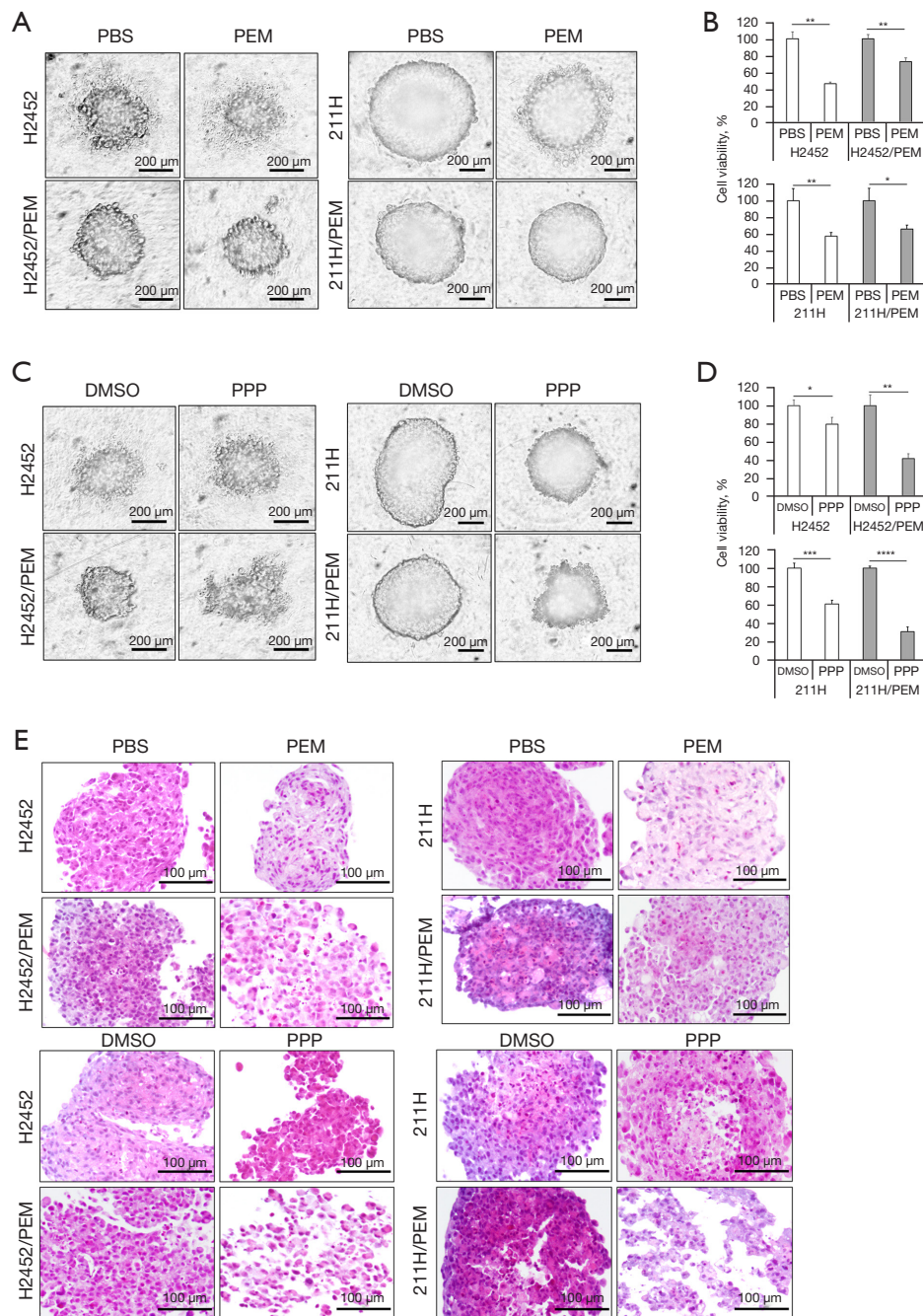


Figure 6 Evaluation of the anticancer efficacy of picropodophyllin (PPP) in 3D malignant pleural mesothelioma (MPM) spheroids and tumor models. (A) Microscopy images (×20) of 3D MPM spheroids. Spheroids were treated with 3 μM pemetrexed (PEM) (H2452 and H2452/PEM for 7 d; 211H and 211H/PEM for 4 d). (B) Cell viability of 3D MPM spheroids treated with 3 μM PEM for 7 (H2452) or 4 (211H) d determined using the CellTiter-Glo 3D Cell Viability Assay. Results represent the mean ± SD, N=3 (biological replicates). P values were calculated using independent sample *t*-test: *, P<0.05; **, P<0.01. (C) Microscopy images (×20) of 3D MPM spheroids. Spheroids were treated with 1 μM PPP for 4 d. (D) Cell viability of 3D MPM spheroids treated with 1 μM PPP for 4 d determined using the CellTiter-Glo 3D Cell Viability Assay. Results represent the mean ± SD, N=3 (biological replicates). P values were calculated using independent sample *t*-test: *, P<0.05; **, P<0.01; ***, P<0.001; ****, P<0.0001. (E) Microscopy images (×10) of 3D MPM tumor tissue models stained with hematoxylin and eosin. Tumors were treated with 3 μM PEM or 1 μM PPP for 4 d.

suggest that the mechanism of action of PPP differs from that of vinorelbine. Chiu *et al.* reported that vinorelbine inhibited the metastatic ability of PEM-resistant lung cancer via inhibiting the ERK–ZEB1 pathway mediating epithelial–mesenchymal transition (49). On the contrary, inhibition of IGF-1R and other RTKs using osimertinib and nintedanib had no anticancer efficacy in PEM-resistant MPM lines. These results indicate the difficulty in targeting RTKs in acquired PEM-resistant MPMs. Moreover, due to a slight decrease in paclitaxel sensitivity of H2452/PEM cells compared with that of H2452 cells, the choice of tubulin inhibitors against PEM-treated MPMs should be made very carefully. Although the action mechanisms of vinorelbine in PEM-resistant cells should be further evaluated, targeting microtubules may be an important therapeutic strategy for MPM with acquired PEM resistance.

Overcoming PEM resistance by targeting essential resistance factors is another plausible way to treat PEM-resistant MPMs. In non-small cell lung cancer, TYMS targeting resulted in the recovery of PEM sensitivity of PEM-resistant cells with TYMS overexpression (25,29,50). However, in this study, almost no efficacy on PEM sensitivity was observed upon TYMS knockdown in 211H/PEM and H2452/PEM cells even though these lines overexpressed TYMS. In addition, IGF-1R inhibition did not affect the PEM sensitivity of the PEM-resistant MPM lines. These results indicate that TYMS overexpression and IGF-1R activation are not essential for PEM resistance in MPMs. The essential factors of PEM resistance in these acquired PEM-resistant lines remain unknown.

For clinical efficacy, oral PPP was tested only in a two-arm trial and the results were not significantly different from those obtained using docetaxel for previously-treated non-small cell lung cancer with a lower incidence of treatment-related grade 3/4 neutropenia (51). In contrast, 50% of PEM-treated patients with progressive MPM had stable disease after vinorelbine treatment (52). Moreover, vinorelbine improved progression-free survival in patients with chemotherapy-treated relapsed MPM compared to the active supportive care alone in a randomized phase II trial (53). Thus, vinorelbine is the most promising candidate for patients with chemotherapy-treated relapsed MPM. Our study highlights that PPP (0.3–0.5 μM) synergized vinorelbine (0.3–10 nM) in two PEM-resistant MPM lines. Vinorelbine combined with PPP would have clinical relevance for patients with MPM after PEM discontinuation.

The main limitations of this study are as follows: only two sets of human MPM cell lines for parental and acquired PEM-resistance were used for the assessment, which is not completely representative of acquired PEM-resistant MPM; additionally, we did not perform *in vivo* experiments using PEM-resistant MPM lines to determine the *in vivo* efficacy and bioequivalence of single and combination treatment with PPP and vinorelbine.

In conclusion, PPP may be more effective against MPMs with acquired PEM resistance than against PEM-naïve MPMs. We found that vinorelbine can potentially be combined with PPP to treat MPMs with acquired PEM resistance.

Acknowledgments

Rong Sun would like to thank the Otsuka Toshimi Scholarship Foundation for support.

Funding: None.

Footnote

Reporting Checklist: The authors have completed the MDAR reporting checklist. Available at <https://tcr.amegroups.com/article/view/10.21037/tcr-21-765/rc>

Data Sharing Statement: Available at <https://tcr.amegroups.com/article/view/10.21037/tcr-21-765/dss>

Conflicts of Interest: All authors have completed the ICMJE uniform disclosure form (available at <https://tcr.amegroups.com/article/view/10.21037/tcr-21-765/coif>). The authors have no conflicts of interest to declare.

Ethical Statement: The authors are accountable for all aspects of the work in ensuring that questions related to the accuracy or integrity of any part of the work are appropriately investigated and resolved.

Open Access Statement: This is an Open Access article distributed in accordance with the Creative Commons Attribution–NonCommercial–NoDerivs 4.0 International License (CC BY-NC-ND 4.0), which permits the non-commercial replication and distribution of the article with the strict proviso that no changes or edits are made and the original work is properly cited (including links to both the formal publication through the relevant DOI and the license). See: <https://creativecommons.org/licenses/by-nc-nd/4.0/>.

References

- Peto J, Hodgson JT, Matthews FE, et al. Continuing increase in mesothelioma mortality in Britain. *Lancet* 1995;345:535-9.
- Bray F, Ferlay J, Soerjomataram I, et al. Global cancer statistics 2018: GLOBOCAN estimates of incidence and mortality worldwide for 36 cancers in 185 countries. *CA Cancer J Clin* 2018;68:394-424.
- Milano MT, Zhang H. Malignant pleural mesothelioma: a population-based study of survival. *J Thorac Oncol* 2010;5:1841-8.
- Pelucchi C, Malvezzi M, La Vecchia C, et al. The Mesothelioma epidemic in Western Europe: an update. *Br J Cancer* 2004;90:1022-4.
- Kameda T, Takahashi K, Kim R, et al. Asbestos: use, bans and disease burden in Europe. *Bull World Health Organ* 2014;92:790-7.
- Baas P, Scherpereel A, Nowak AK, et al. First-line nivolumab plus ipilimumab in unresectable malignant pleural mesothelioma (CheckMate 743): a multicentre, randomised, open-label, phase 3 trial. *Lancet* 2021;397:375-86.
- Waterhouse DM, Nwokeji ED, Boyd M, et al. Treatment patterns and outcomes of patients with advanced malignant pleural mesothelioma in a community practice setting. *Future Oncol* 2021;17:2439-48.
- Taylor P, Castagneto B, Dark G, et al. Single-agent pemetrexed for chemo-naïve and pretreated patients with malignant pleural mesothelioma: results of an International Expanded Access Program. *J Thorac Oncol* 2008;3:764-71.
- Bueno R, Stawiski EW, Goldstein LD, et al. Comprehensive genomic analysis of malignant pleural mesothelioma identifies recurrent mutations, gene fusions and splicing alterations. *Nat Genet* 2016;48:407-16.
- Hmeljak J, Sanchez-Vega F, Hoadley KA, et al. Integrative Molecular Characterization of Malignant Pleural Mesothelioma. *Cancer Discov* 2018;8:1548-65.
- Hinz TK, Heasley LE. Translating mesothelioma molecular genomics and dependencies into precision oncology-based therapies. *Semin Cancer Biol* 2020;61:11-22.
- Stapelberg M, Gellert N, Swettenham E, et al. α -Tocopheryl Succinate Inhibits Malignant Mesothelioma by Disrupting the Fibroblast Growth Factor Autocrine Loop. *J Biol Chem* 2005;280:25369-76.
- Poulikakos PI, Xiao GH, Gallagher R, et al. Re-expression of the tumor suppressor NF2/merlin inhibits invasiveness in mesothelioma cells and negatively regulates FAK. *Oncogene* 2006;25:5960-8.
- Servais EL, Colovos C, Rodriguez L, et al. Mesothelin overexpression promotes mesothelioma cell invasion and MMP-9 secretion in an orthotopic mouse model and in epithelioid pleural mesothelioma patients. *Clin Cancer Res* 2012;18:2478-89.
- Pinton G, Manente AG, Murer B, et al. PARP1 inhibition affects pleural mesothelioma cell viability and uncouples AKT/mTOR axis via SIRT1. *J Cell Mol Med* 2013;17:233-41.
- Hassan R, Kindler HL, Jahan T, et al. Phase II clinical trial of amatumimab, a chimeric antimesothelin antibody with pemetrexed and cisplatin in advanced unresectable pleural mesothelioma. *Clin Cancer Res* 2014;20:5927-36.
- Fennell DA, Baas P, Taylor P, et al. Maintenance Defactinib Versus Placebo After First-Line Chemotherapy in Patients With Merlin-Stratified Pleural Mesothelioma: COMMAND—A Double-Blind, Randomized, Phase II Study. *J Clin Oncol* 2019;37:790-8.
- Kalra N, Zhang J, Yu Y, et al. Efficacy of anti-insulin-like growth factor I receptor monoclonal antibody cixutumumab in mesothelioma is highly correlated with insulin growth factor-I receptor sites/cell. *Int J Cancer* 2012;131:2143-52.
- Simpson A, Petnga W, Macaulay VM, et al. Insulin-Like Growth Factor (IGF) Pathway Targeting in Cancer: Role of the IGF Axis and Opportunities for Future Combination Studies. *Target Oncol* 2017;12:571-97.
- Whitson BA, Jacobson BA, Frizelle S, et al. Effects of Insulin-Like Growth Factor-1 Receptor Inhibition in Mesothelioma. *Ann Thorac Surg* 2006;82:996-1001.
- McKian KP, Haluska P. Cixutumumab. *Expert Opin Investig Drugs* 2009;18:1025-33.
- Kai K, D'Costa S, Sills RC, et al. Inhibition of the insulin-like growth factor 1 receptor pathway enhances the antitumor effect of cisplatin in human malignant mesothelioma cell lines. *Cancer Lett* 2009;278:49-55.
- Girnita A, Girnita L, del Prete F, et al. Cyclolignans as inhibitors of the insulin-like growth factor-1 receptor and malignant cell growth. *Cancer Res* 2004;64:236-42.
- [dataset] DepMap, Broad; 2021. DepMap 21Q3 Public, Version 2. DOI: 10.6084/M9.FIGSHARE.15160110.V2.
- Tanino R, Tsubata Y, Harashima N, et al. Novel drug-resistance mechanisms of pemetrexed-treated non-small cell lung cancer. *Oncotarget* 2018;9:16807-21.

26. Nakagawa K, Kudoh S, Matsui K, et al. A phase I study of pemetrexed (LY231514) supplemented with folate and vitamin B12 in Japanese patients with solid tumours. *Br J Cancer* 2006;95:677-82.
27. Curtin NJ, Hughes AN. Pemetrexed disodium, a novel antifolate with multiple targets. *Lancet Oncol* 2001;2:298-306.
28. Chattopadhyay S, Moran RG, Goldman ID. Pemetrexed: biochemical and cellular pharmacology, mechanisms, and clinical applications. *Mol Cancer Ther* 2007;6:404-17.
29. Ozasa H, Oguri T, Uemura T, et al. Significance of thymidylate synthase for resistance to pemetrexed in lung cancer. *Cancer Sci* 2010;101:161-6.
30. Chen J, Wang Z, Gao S, et al. Human drug efflux transporter ABCB5 confers acquired resistance to pemetrexed in breast cancer. *Cancer Cell Int* 2021;21:136.
31. Ekman S, Harmenberg J, Frödin JE, et al. A novel oral insulin-like growth factor-1 receptor pathway modulator and its implications for patients with non-small cell lung carcinoma: A phase I clinical trial. *Acta Oncol* 2016;55:140-8.
32. Sperandio S, de Belle I, Bredesen DE. An alternative, nonapoptotic form of programmed cell death. *Proc Natl Acad Sci U S A* 2000;97:14376-81.
33. Wu X, Sooman L, Wickström M, et al. Alternative cytotoxic effects of the postulated IGF-1R inhibitor picropodophyllin in vitro. *Mol Cancer Ther* 2013;12:1526-36.
34. Waraky A, Akopyan K, Parrow V, et al. Picropodophyllin causes mitotic arrest and catastrophe by depolymerizing microtubules via insulin-like growth factor-1 receptor-independent mechanism. *Oncotarget* 2014;5:8379-92.
35. Park HS, Han JH, Jung SH, et al. Anti-apoptotic effects of autophagy via ROS regulation in microtubule-targeted and PDGF-stimulated vascular smooth muscle cells. *Korean J Physiol Pharmacol* 2018;22:349-60.
36. Mitsiades CS, Mitsiades NS, McMullan CJ, et al. Inhibition of the insulin-like growth factor receptor-1 tyrosine kinase activity as a therapeutic strategy for multiple myeloma, other hematologic malignancies, and solid tumors. *Cancer Cell* 2004;5:221-30.
37. Klinakis A, Szabolcs M, Chen G, et al. IGF1R as a therapeutic target in a mouse model of basal-like breast cancer. *Proc Natl Acad Sci U S A* 2009;106:2359-64.
38. Zha J, Lackner MR. Targeting the insulin-like growth factor receptor-1R pathway for cancer therapy. *Clin Cancer Res* 2010;16:2512-7.
39. Fuentes-Baile M, Ventero MP, Encinar JA, et al. Differential Effects of IGF-1R Small Molecule Tyrosine Kinase Inhibitors BMS-754807 and OSI-906 on Human Cancer Cell Lines. *Cancers (Basel)* 2020;12:3717.
40. Mc Gee MM. Targeting the Mitotic Catastrophe Signaling Pathway in Cancer. *Mediators Inflamm* 2015;2015:146282.
41. Bröker LE, Kruyt FA, Giaccone G. Cell death independent of caspases: a review. *Clin Cancer Res* 2005;11:3155-62.
42. Miyayama A, Masuda M, Tsuta K, et al. Hippo pathway gene mutations in malignant mesothelioma: revealed by RNA and targeted exon sequencing. *J Thorac Oncol* 2015;10:844-51.
43. Sneddon S, Creaney J. BAP1 mutations in mesothelioma: advances and controversies. *Curr Pulmonol Rep* 2016;5:13-9.
44. Carbone M, Harbour JW, Brugarolas J, et al. Biological Mechanisms and Clinical Significance of BAP1 Mutations in Human Cancer. *Cancer Discov* 2020;10:1103-20.
45. Singh A, Luo J, Busacca S, et al. Loss of BAP1/BRCA1 counteracts spindle assembly checkpoint activation by the anti-mesothelin antibody drug-conjugate anetumab ravtansine. In: Proceedings of the Annual Meeting of the American Association for Cancer Research 2020; 2020 Apr 27-28 and Jun 22-24; Philadelphia, PA.
46. Busacca S, O'Regan L, Singh A, et al. BRCA1/MAD2L1 Deficiency Disrupts the Spindle Assembly Checkpoint to Confer Vinorelbine Resistance in Mesothelioma. *Mol Cancer Ther* 2021;20:379-88.
47. Furth N, Aylon Y. The LATS1 and LATS2 tumor suppressors: beyond the Hippo pathway. *Cell Death Differ* 2017;24:1488-501.
48. Kindler HL, Ismaila N, Armato SG 3rd, et al. Treatment of Malignant Pleural Mesothelioma: American Society of Clinical Oncology Clinical Practice Guideline. *J Clin Oncol* 2018;36:1343-73.
49. Chiu LY, Hsin IL, Yang TY, et al. The ERK-ZEB1 pathway mediates epithelial-mesenchymal transition in pemetrexed resistant lung cancer cells with suppression by vinca alkaloids. *Oncogene* 2017;36:242-53.
50. Takezawa K, Okamoto I, Okamoto W, et al. Thymidylate synthase as a determinant of pemetrexed sensitivity in non-small cell lung cancer. *Br J Cancer* 2011;104:1594-601.
51. Bergqvist M, Holgersson G, Bondarenko I, et al. Phase II randomized study of the IGF-1R pathway modulator AXL1717 compared to docetaxel in patients with previously treated, locally advanced or metastatic non-

- small cell lung cancer. *Acta Oncol* 2017;56:441-7.
52. Zucali PA, Perrino M, Lorenzi E, et al. Vinorelbine in pemetrexed-pretreated patients with malignant pleural mesothelioma. *Lung Cancer* 2014;84:265-70.
53. Fennell DA, Casbard AC, Porter C, et al. A randomized phase II trial of oral vinorelbine as second-line therapy for patients with malignant pleural mesothelioma. *J Clin Oncol* 2021;39:8507.

Cite this article as: Sun R, Tanino R, Tong X, Haque EF, Amano Y, Isobe T, Tsubata Y. Picropodophyllin inhibits the growth of pemetrexed-resistant malignant pleural mesothelioma via microtubule inhibition and IGF-1R-, caspase-independent pathways. *Transl Lung Cancer Res* 2022;11(4):543-559. doi: 10.21037/tlcr-21-765

Appendix 1 Supplementary Methods

Immunoblotting analysis for protein expression

Cells were harvested at less than 70% confluence. The cells were then centrifuged at $800 \times g$ for 5 min, washed with PBS, and lysed in M-PER Mammalian Protein Extraction Reagent (Thermo Fisher Scientific, Waltham, MA, USA) containing 1% Halt Protease Inhibitor Cocktail (Thermo Fisher Scientific) and 1% Phosphatase Inhibitor Cocktail (Nacalai Tesque, Kyoto, Japan). The lysate was centrifuged at $14,000 \times g$ for 15 min. The supernatant was used as the protein lysate. The protein concentration in the lysate was measured using the Pierce Coomassie Plus Assay Kit (Thermo Fisher Scientific). Samples with an equal quantity of proteins were prepared by mixing the lysate with 25% Bolt LDS Sample Buffer (Thermo Fisher Scientific) and 10% Bolt Sample Reducing Agent (Thermo Fisher Scientific), and each sample was adjusted to an equal volume by adding distilled water and incubated at $95 \text{ }^\circ\text{C}$ for 5 min. The samples were electrophoresed on a Tris-glycine gel set in a Bolt Mini Gel Tank (Thermo Fisher Scientific). The proteins in the gel were transferred to a ClearTrans Nitrocellulose Membrane, $0.2 \text{ }\mu\text{m}$ (Fujifilm Wako, Osaka, Japan), using a Mini Blot Module (Thermo Fisher Scientific). The membrane was rinsed with TBS and blocked with 5% non-fat skim milk or 2% ECL Prime Blocking Reagent (Cytiva, Marlborough, MA, USA) in 0.1% Tween 20 (Nacalai Tesque) in TBS (TBS-T) for 60 min, and incubated with a primary antibody diluted in 10% Blocker BSA in TBS (37520; Thermo Fisher Scientific) in TBS-T overnight at $4 \text{ }^\circ\text{C}$. The membrane was washed thrice with TBS-T for 10 min and incubated with a secondary antibody diluted in 5% non-fat skim milk in TBS-T. The membrane was washed thrice with TBS-T for 10 min, and protein bands were visualized with ECL Select Western Blotting Detection Reagent (Cytiva) using Amersham ImageQuant 800 (Cytiva). The primary antibodies used for immunoblotting are listed in Table S3. ECL Anti-Rabbit IgG HRP-Linked Whole Ab Donkey (NA934; Cytiva, RRID: AB_772206) or ECL Anti-Mouse IgG HRP-Linked Whole Ab Sheep (NA931; Cytiva, RRID: AB_772210) were used as the secondary antibodies.

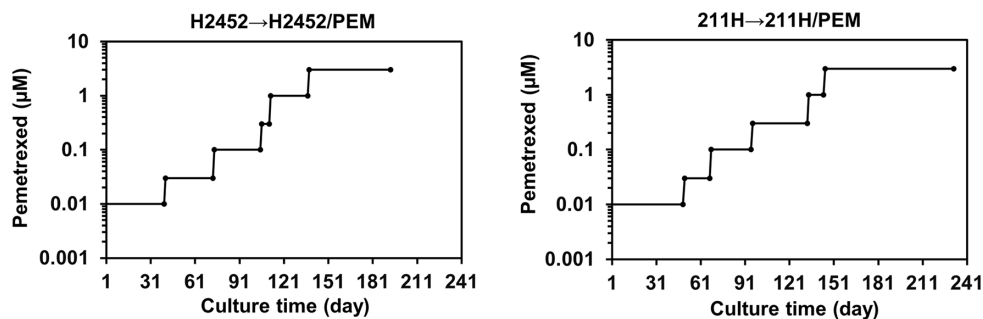
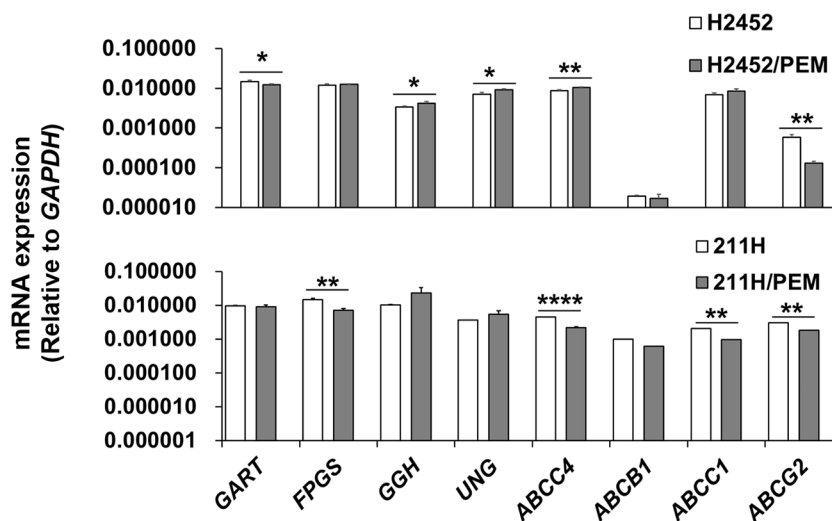
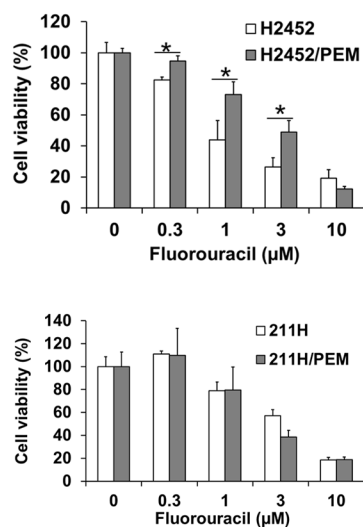


Figure S1 Establishment of two acquired pemetrexed-resistant MPM cell lines. H2452/PEM and 211H/PEM were established from human MPM cell lines H2452 and 211H by continuous exposure to pemetrexed. Dots indicate the pemetrexed concentration in the culture medium and the time point of pemetrexed concentration increase.

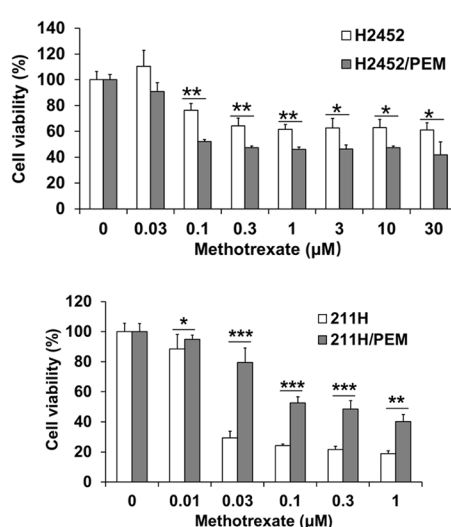
A



B



C



D

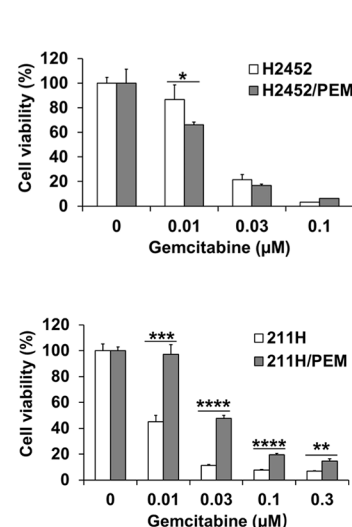


Figure S2 Evaluation of multidrug resistance to folate-related and anti-cytidine drugs of pemetrexed-resistant MPM cell lines. A, mRNA expression of genes related to folate and multidrug resistance proteins in MPM cells was detected by quantitative reverse-transcription PCR. Results represent the mean + SD. N = 3 (biological replicates). P values were calculated using the independent-sample *t*-test, **P*<0.05, ***P*<0.01, *****P*<0.0001. B, Viability of MPM cells treated with the indicated concentrations of fluorouracil for 120 h determined using the WST-8 assay. Results represent the mean + SD, N = 3 (biological replicates). P values were calculated using the independent-sample *t*-test, **P*<0.05. C, Viability of MPM cells treated with the indicated concentrations of methotrexate for 96 (H2452) or 48 (211H) h determined using the WST-8 assay. Results represent the mean + SD. N = 3 (biological replicates). P values were calculated using the independent-sample *t*-test, **P*<0.05, ***P*<0.01, ****P*<0.001. D, Viability of MPM cells treated with the indicated concentrations of gemcitabine for 144 (H2452) or 48 (211H) h was determined using the WST-8 assay. Results represent the mean + SD, N = 3 (biological replicates). P values were calculated using the independent-sample *t*-test, **P*<0.05, ***P*<0.01, ****P*<0.001, *****P*<0.0001.

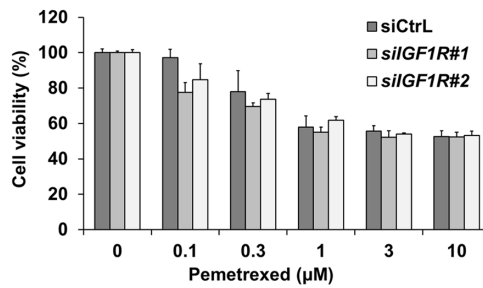


Figure S3 Viability of *IGF1R* knockdown pemtetrexed-resistant MPM cells treated with the indicated concentration of pemtetrexed for 96 (H2452/PEM) h. Negative control of siRNA transfection (siCtrl) was used. Results represent the mean + SD, N = 3 (biological replicates).

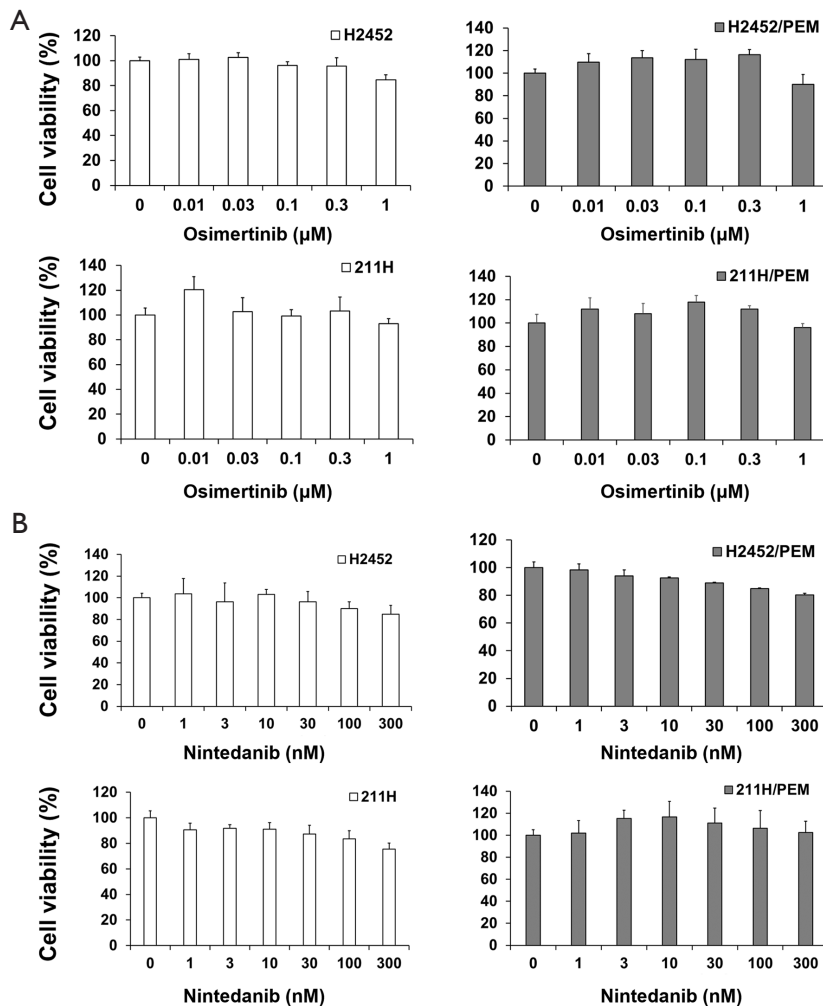


Figure S4 Acquired pemtetrexed-resistant MPM cells were not sensitive to the other TKIs. (A) Viability of pemtetrexed-resistant MPM cells treated with the indicated concentration of osimertinib for 120 (H2452) or 72 (211H) h determined using WST-8 assay. Results represent the mean + SD, N = 3 (biological replicates). (B) Viability of PEM-resistant MPM cells treated with the indicated concentrations of nintedanib for 144 (H2452) or 48 (211H) h determined using WST-8 assay. Results represent the mean + SD, N = 3 (biological replicates).

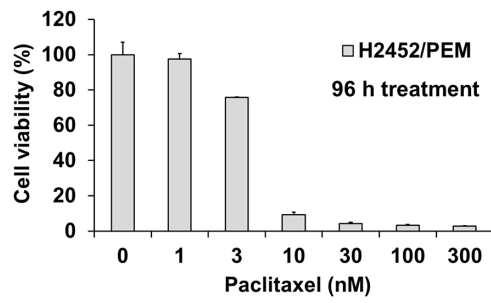


Figure S5 Viability of H2452/PEM treated with indicated concentrations of paclitaxel for 96 h determined using WST-8 assay. Results represent the mean + SD, N = 3 (biological replicates).

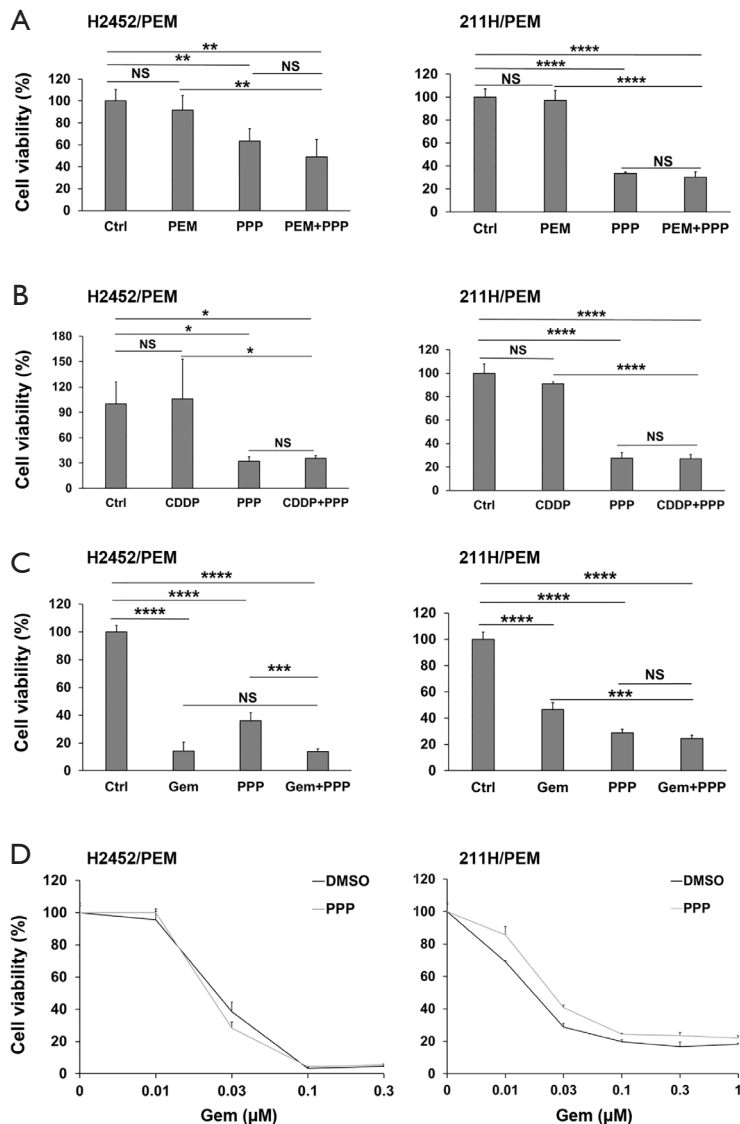


Figure S6 Assessment of picropodophyllin (PPP) plus other chemotherapeutic drugs on acquired pemetrexed (PEM) resistant MPM cells. (A) Viability of PEM-resistant MPM cells treated with 3 μM PEM without or with 0.5 μM PPP for H2452/PEM or 0.4 μM PPP for 211H/PEM and the same volume of DMSO as a control (Ctrl) for H2452/PEM (144 h) or 211H/PEM (96 h) determined using WST-8 assay. Results represent the mean + SD, N = 3 (biological replicates). P values were calculated using one-way ANOVA analysis and a post-hoc Dunnett's test, **P<0.01, ****P<0.0001, NS, not significant. (B) Viability of PEM-resistant MPM cells treated with 1 μM (H2452/PEM) or 0.7 μM (211H/PEM) cisplatin (CDDP) without or with 0.5 μM PPP for H2452/PEM or 0.4 μM PPP for 211H/PEM and the same volume of DMSO as a control for H2452/PEM (144 h) or 211H/PEM (96 h) determined using WST-8 assay. Results represent the mean + SD, N = 3 (biological replicates). P values were calculated using one-way ANOVA analysis and a post-hoc Dunnett's test, *P<0.05, ****P<0.0001, NS, not significant. (C) Viability of PEM-resistant MPM cells treated with 0.03 μM (H2452/PEM) or 0.01 μM (211H/PEM) gemcitabine (Gem) without or with 0.5 μM PPP for H2452/PEM or 0.4 μM PPP for 211H/PEM and the same volume of DMSO as a control for H2452/PEM (144 h) or 211H/PEM (96 h) determined using WST-8 assay. Results represent the mean + SD, N = 3 (biological replicates). P values were calculated using one-way ANOVA analysis and a post-hoc Dunnett's test, ***P<0.001, ****P<0.0001, NS, not significant. (D) Viability of PEM-resistant MPM cells treated with indicated concentrations of Gem without or with 0.5 μM PPP for H2452/PEM or 0.3 μM PPP for 211H/PEM and the same volume of DMSO as a control for H2452/PEM (144 h) or 211H/PEM (48 h) determined using WST-8 assay. Results represent the mean + SD, N = 3 (biological replicates).

Table S1 Variants and copy number variations of tumor-associated genes

Gene	H2452	MSTO-211H
<i>CDKN2A</i>	loss	loss
<i>CDKN2B</i>	loss	loss
<i>BAP1</i>	A95D	wild type
<i>LATS1</i>	wild type	loss
<i>LATS2</i>	wild type	M785_L798del / M785I
<i>MYC</i>	wild type	Copy number amplification

Table S2 The primer sequences for quantitative PCR.

Gene	Forward primer (5' to 3')	Reverse primer (5' to 3')
<i>DHFR</i>	CCATACTGCTGAGATACAGGGAAAT	ACACAGGACAGGGAGCTGACA
<i>GART</i>	CAATGGCAGCCCGAGTACTTA	GACATGATGAGACTGTGCAAGTTTC
<i>TYMS</i>	CACACTTTGGGAGATGCACATATT	TTCGAAGAATCCTGAGCTTTGG
<i>ABCB1</i>	AGGCCAACATACATGCCTTC	CCACCAGAGAGCTGAGTTCC
<i>ABCC1</i>	CCTGTTCAACGTCATTGGTG	AGCCACGTAGAACCTCTGGA
<i>ABCC4</i>	TCTGGACCATCCGGGCATAC	TGGTGGTGGGCGTTTCTGAT
<i>ABCC5</i>	CCTGCAGTACAGCTTGTGTTAGTG	GACACCGTTCCGGTAATTCAAT
<i>FPGS</i>	CTATGCCGTCTTCTGCCCTAAC	ACCTGGTCCAGTGTCACTGTGA
<i>GGH</i>	GCGAGCCTCGAGCTGTCTA	AATATTCCGATGATGGGCTTCTT
<i>SLC19A1</i>	CATCGCCACCTTTCAGATT	TGGCAAAGAACGTGTTGAC
<i>IGF1R</i>	TGGTGGAGAACGACCATATCC	CGATTAAGTGAAGAGGAGTTCTGA
<i>PXN</i>	ACGTCTACAGCTTCCCCAACAA	AGCAGGCGGTCCGAGTTCA
<i>ITGB1</i>	CATCTGCGAGTGTGGTGTCT	AAGGCTCTGCACTGAACACA
<i>GAB1</i>	ATCAGAAACGCCAGCGAAGA	TCAGATACCACAAAGCACCA
<i>GAB2</i>	ACAGTACCTACGACCTCCCC	CTGGGCGTCTTGAAGGTGTA
<i>JAK1</i>	AGACTTGTGAATACGTTAAAAGAAGGA	AAAGCTTGTCCGATTGGATG
<i>ERBB2</i>	TGTGACTGCCTGTCCCTACAA	CCAGACCATAGCACACTCGG
<i>PDGFRB</i>	GCACCGAAACAAACACACCTT	ATGTAACCACCGTCGCTCTC
<i>MET</i>	CCATCCAGTGTCTCCAGAAGTG	TTCCCAGTGATAACCAGTGTGTAG
<i>AXL</i>	TACCGCCAGGGACGTATCGC	CCAGCACCGCGACATCAAGG
<i>GAS6</i>	TGGCGCGGAATCTGGTCATC	GAAGCACTGCATCCTCGTGTTG
<i>EPHA2</i>	CCGGCTACACTGCCATCGAG	GCCCAGCATCCCTGGTCATC
<i>TYRO3</i>	AACATCTTGGGCCAGCTGTCTG	GATTTGGTCAGTCCGGGCTTC
<i>TWIST1</i>	CATGTCCGCGTCCCCTAG	TGTCCATTTTCTCCTTCTCTGG
<i>GAPDH</i>	GCACCGTCAAGGCTGAGAAC	TGGTGAAGACGCCAGTGGA

Table S3 The information of primary antibodies for immunoblotting.

Target protein	Company	Catalog number	RRID
IGF1R β	Cell Signaling	9750	AB_10950969
Phospho-IGF1R (Y1165+Y1166)	Bioss	bs-5449R	AB_11096251
Akt1/2/3	Santa Cruz	sc-8312	AB_671714
Phospho-Akt1/2/3 (S473)	Cell Signaling	4060	AB_2315049
Erk1/2	Cell Signaling	4695	AB_390779
Phospho-Erk1/2 (T202/Y204)	Cell Signaling	4370	AB_2315112
Thymidylate synthase	Agilent	M3614	AB_2210727
DHFR	Abnova	H00001719-M01	AB_565642
SLC19A1	GeneTex	GTX46753	AB_11174097
ABCC5	GeneTex	GTX81163	AB_11164308
Chk2	Cell Signaling	6334	AB_11178526
Phospho-Chk2 (T68)	Cell Signaling	2197	AB_2080501
PARP1	Cell Signaling	9532	AB_659884
alpha-Tubulin	Santa Cruz	sc-5286	AB_628411
GAPDH	Cell Signaling	8884	AB_11129865

IGF1R, insulin-like growth factor 1 receptor; DHFR, dihydrofolate reductase; SLC19A1, reduced folate transporter; ABCC5, multidrug resistance-associated protein 5; Chk2, serine/threonine-protein kinase Chk2; PARP1, poly(ADP-ribose) polymerase 1; GAPDH, glyceraldehyde-3-phosphate dehydrogenase.